ISSN 0965-5441, Petroleum Chemistry, 2016, Vol. 56, No. 3, pp. 253–258. © Pleiades Publishing, Ltd., 2016.
Original Russian Text © O.A. Ponomareva, A.A. Mal'tseva, A.A. Maerle, L.I. Rodionova, V.S. Pavlov, I.V. Dobryakova, M.V. Belova, I.I. Ivanova, 2016, published in Neftekhimiya, 2016, Vol. 56, No. 3, pp. 271–276.

Production of Isobutylene from Acetone over Micro–Mesoporous Catalysts

O. A. Ponomareva[a, b], A. A. Mal'tseva[a], A. A. Maerle[a], L. I. Rodionova[a], V. S. Pavlov[b], I. V. Dobryakova[a], M. V. Belova[a], I. I. Ivanova[a, b]

[a] *Faculty of Chemistry, Moscow State University, Moscow, Russia*

[b] *Topchiev Institute of Petrochemical Synthesis, Russian Academy of Sciences, Moscow, Russia*

e-mail: oaponomareva@phys.chem.msu.ru

Received November 16, 2015

Abstract—The production of isobutylene from acetone over micro–mesoporous catalysts with different mesopore contents, which have been prepared using hydrothermal recrystallization of mordenite (MOR) zeolite modified with cesium acetate by incipient wetness impregnation, has been studied. It has been shown that cesium is inserted into the cation positions during the modification, at the same time the number of Brønsted acid sites in the samples decreased. It has been found that an increase in the content of mesopores in the catalyst leads to an increase in the initial rates of acetone conversion and isobutylene formation as a result of removing diffusion limitations. Brønsted acid sites have been shown to be preferable for the selective production of isobutylene from acetone. Micro–mesoporous materials operate more stably as compared to microporous materials.

Keywords: acetone, isobutylene, micro–mesoporous catalysts, cesium, mordenite

DOI: 10.1134/S0965544116030075

Isobutylene is a valuable product for industrial use; it is feedstock for high-volume production processes for the manufacture of isoprene, methyl methacrylate, *tert*-butyl methyl ether, and synthetic rubbers. Currently, isobutylene is mostly obtained by isolating it from the butane–butene fraction produced by petroleum refining, as well as from natural gas or via the dehydration of isobutanol. However, it should be realized that energy resources are gradually depleting, while the demand for isobutylene exceeds the supply and the need for its production continuously increases; thus, there is a necessity of searching for alternative processes of its production. Its synthesis from acetone, which, in turn, is formed in large quantities as a byproduct in large-scale industrial processes, such as the production of phenol and biobutanol, can become a possible solution of this problem. In addition, acetone can be produced during the processing of nonedible biomass or via the enzymatic breakdown of sewage sludge [1].

Earlier, the transformations of acetone into isobutylene have been studied over oxide catalysts supported on silica gel (WO_3/SiO_2 [2] and Al_2O_3/SiO_2 [3]); mixed oxides $Zn_xZr_yO_z$ [4]; molecular sieve SAPO-34 [5]; zeolites BEA [6, 7–9], MFI [1, 10–13], *X*, and *Y* [14]; and mesoporous material MCM-41 [15]. Generally, the experiments were conducted at high temperatures (300–500°C) and atmospheric pressure.

Acetone conversion is accompanied by rapid deactivation of catalysts, modifying alkali metals contributes to the stability of their work. Iit was found [7] that the most efficient are modifiers cesium and rubidium.

The conversion of acetone proceeds via the aldol condensation to form diacetone alcohol, which further decomposes to give isobutylene and acetic acid:

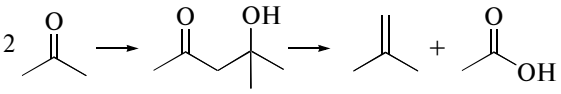

Resulting isobutylene undergoes further transformations, resulting in aliphatic and aromatic hydrocarbons, as well as condensation products. The dehydration of diacetone alcohol gives mesityl oxide [16].

Micro–mesoporous molecular sieves, which combine high acidity and unique molecular stereoselectivity of zeolites with the transport characteristics of mesoporous materials, are promising heterogeneous catalysts for the transformation of organic molecules.

Among various methods for the synthesis of micro–mesoporous materials, recrystallization is the simplest, reproducible method that makes it possible to control the amount and size of mesopores in the material. To date, it has become known that micro–mesoporous structures with various micropore to mesopore ratios can be obtained using this quite simple procedure applicable to zeolites of any structural

type [17]. The recrystallization procedure includes partial dissolution of zeolite in an alkaline solution containing a structure-directing agent, which can be selected from a number of different surfactants.

It is assumed that partial degradation of the zeolite structure and removal of zeolitic fragments, in the place of which mesopores are formed, occurs at the dissolution stage. The next stage involves the reassembly of the dispersed particles into a mesoporous phase that, depending on the degree of dissolution of initial zeolite, can simply cover its surface (RZEO-1), form micro–mesoporous composites (RZEO-2), or create a mesoporous material with small fragments of zeolitic particles into embedded its walls (RZEO-3) [17].

In this work, we first studied the conversion of acetone into isobutylene over micro–mesoporous catalysts with different mesopore contents that had been prepared via the recrystallization of mordenite (MOR) and examined the effects of porosity characteristics and cesium modification of the catalyst on its physicochemical and catalytic properties.

EXPERIMENTAL

Mordenite (MOR) with a silica ratio of $SiO_2/Al_2O_3 = 97$ (Zeolyst, trade name CBV 90A) was used as initial zeolite. Mesoporous aluminosilicate MCM-41 with $SiO_2/Al_2O_3 = 100$ was prepared from an aluminosilicate gel via hydrothermal synthesis at 140°C for 24 h using cetyltrimethylammonium bromide as the template. After crystallization, the obtained mesoporous material was washed with water, dried at 100°C, and calcined at 550°C in a flow of air for 24 h in order to remove the organic template.

The recrystallization of MOR was conducted by the partial dissolution of zeolite in an alkali solution with the subsequent hydrothermal treatment in the presence of cetyltrimethylammonium bromide according to the procedure described in [18]. The degree of recrystallization was varied by changing the alkali concentration. In order to obtain materials RM-1, RM-2, and RM-3 with different micropore and mesopore contents, alkali to zeolite ratios of 3, 5, and 10 mmol(NaOH)/g(MOR) were used, respectively. The prepared samples were washed to free of the template and calcined in air at 550°C for 24 h. The synthesized MCM-41 and micro–mesoporous aluminosilicates were subjected to triple ion exchange with ammonium nitrate and subsequent calcining in a flow of air at 550°C for 6 h to prepare the H-forms. The catalysts were modified with cesium by incipient wetness impregnation with a cesium acetate solution to have a metal loading of 3 wt %.

The chemical composition of the obtained materials was determined using X-ray fluorescence analysis on a Thermo Scientific ARL Perform'X instrument equipped with a 3.5-kW rhodium tube. X-ray diffraction (XRD) patterns were recorded on a Bruker D2 PHASER diffractometer (Cu$K\alpha$ radiation) in the angular range of $5° < 2\theta < 50°$. Small-angle X-ray scattering (SAXS) patterns were recorded in the angular range of $1.5° < 2\theta < 5°$. The diffractograms were processed using the Bruker software package diffrac.EVA. Phases were identified according to the ICDD PDF2 database.

Electron microscope (TEM) images of the samples were obtained on a Jeol JEM 2010 transmission electron microscope with a 200-keV electron beam.

Low-temperature nitrogen adsorption-desorbtion isotherms were obtained on a Micromeritics ASAP2000 automatic porosimeter. The micropore volume was determined using the *t*-plot method. The pore volume, which takes into account adsorption in micropores and mesopores and on the external surface, was calculated from the amount of nitrogen sorbed at a relative pressure of $p/p_0 = 0.95$.

The acid properties of the samples were studied using the technique of temperature-programmed desorption of ammonia (NH_3 TPD) on a USGA-101 multipurpose sorption gas analyzer. A weighed portion of the sample was placed in a quartz reactor, heated in a helium flow to 550°C at a heating rate of 10°C/min, calcined at this temperature for 1 h in a helium flow, and then cooled to 60°C. Saturation with ammonia was conducted for 15 min in a flow of dry NH_3/N_2 (1 : 1) mixture. Physisorbed ammonia was removed at 100°C in a flow of dry helium for 1 h. After that the sample was cooled to 60°C in a flow of dry helium (flow rate of 30 mL/min), and the reactor temperature was linearly raised to 800°Cat a rate of 8°C/min. The change in the thermal conductivity of the flow was recorded using a katharometer.

IR spectra were recorded on a Bruker Vector 22 instrument equipped with a deuterated triglycidyl sulfate (DTGS) detector with the optical resolution of 4 cm^{-1} in the range of 4000–400 cm^{-1}. The catalysts were activated in the IR cell at 400°C and 10^{-5} torr for 2 h. The adsorption of pyridine (Py) was conducted at 200°C for 30 min with the subsequent evacuation at 200°C for 15 min. The obtained IR spectra were processed using the software package OMNIC ESP Version 6.0.

The conversion of acetone into isobutylene was studied in a flow reactor at atmospheric pressure using dilution of the reaction mixture with nitrogen (20 mL/min), a temperature 500°C, and a feedstock weight hourly space velocity (WHSV) of 2 to 72 h^{-1}. Liquid and gaseous reaction products were determined by chromatographic analysis on a Chromatec Analytic Kristall 2000M gas chromatograph with a flame ionization detector (FID) and an SE-30-coated capillary column using nitrogen as a carrier gas. To determine CO_2 and light C_1 and C_2 hydrocarbons, gaseous samples were also analyzed on the Kristall 2000M chromatograph using a thermal conductivity detector, and a packed Porapak-Q column, hydrogen as a carrier gas. The products were identified using authentic organic substances and the coupled gas chromatogra-

Table 1. Physicochemical properties of catalysts

Sample name	V_{total}, cm^3/g	V_{micr}, cm^3/g	V_{micr}/V_{total}	SiO_2/Al_2O_3	Metal content, wt %	$a_0(NH_3)$, μmol/g	$a_0(NH_3)$/ μmol Al
MOR	0.24	0.16	0.66	97	–	436	1.3
Cs/MOR	0.25	0.17	0.68	98	3.0	182	0.5
RM-1	0.34	0.13	0.38	92	–	376	1.3
Cs/RM-1	0.33	0.30	0.39	92	3.0	119	0.4
RM-2	0.45	0.09	0.20	94	–	319	.0.9
Cs/RM-2	0.45	0.06	0.13	94	3.0	132	0.3
RM-3	0.80	0.03	0.04	96	–	276	0.8
Cs/RM-3	0.67	0	0	96	3.0	63	0.2
MCM-41	0.84	0	0	100	–	267	0.8
Cs/MCM-41	0.86	0	0	100	3.0	342	1.0

phy–mass spectrometry technique with a Thermo Trace GC Ultra chromatograph and a Thermo DSQ II mass spectrometer on a 50-m fused silica capillary column with the Ultra 1 nonpolar liquid phase.

The catalytic properties of the samples were characterized by the initial reaction rate, acetone conversion, and selectivity for the products. The initial reaction rate was determined by differentiating the initial part of kinetic curves that represented the conversion of the reactant as a function of space time.

RESULTS AND DISCUSSION

Physicochemical Properties of Catalysts

The conversion of acetone into isobutylene was studied over cesium-containing micro–mesoporous catalysts prepared by the recrystallization of mordenite and characterized by different contributions of micropores and mesopores. The physicochemical properties of the obtained samples are presented in Table 1.

The XRD, SAXS,, low-temperature nitrogen adsorption-desorbtion, and TEM data obtained for samples RM-1, RM-2, and RM-3 are similar to those presented in the review [17] (not given in this paper) and show that the materials prepared by recrystallization of the initial mordenite zeolite are as follows: RM-1 is zeolite crystals partially covered with a mesoporous phase, RM-2 is a micro–mesoporous zeolite/MCM-41 nanocomposite, and RM-3 is a mesoporous material with zeolite fragments embedded in its walls.

The modification with cesium alters neither morphology nor the porosity characteristics of the samples (Table 1).

Figure 1 presents acidity spectra for MOR, MCM-41, and micro–mesoporous samples. Mordenite is characterized by a curve with two maximums at 170 and 460°C. The low-temperature maximum corresponds to weak acid sites and physisorbed ammonia molecules, and the high-temperature maximum is due to strong acid sites. The curve for the mesoporous material MCM-41 exhibits one characteristic peak at 290°C, which corresponds to medium-strength acid sites. An increase in the degree of recrystallization leads to a decrease in the total number of acid sites and a decrease in their strength, as indicated by the shift of the maximum of the high-temperature peak towards lower temperatures. The differences in the amount of acid sites between the micro–mesoporous materials with the same SiO_2/Al_2O_3 ratio can be explained by the fact that during the formation of the mesoporous phase, part of aluminum atoms are incorporated into the walls of the material and become inaccessible to ammonia molecules.

This assumption is confirmed by the fact that the calculated ratio of the amount of ammonia desorbed from the samples to the amount of aluminum in them decreases on passing from mordenite to MCM-41 (Table 1).

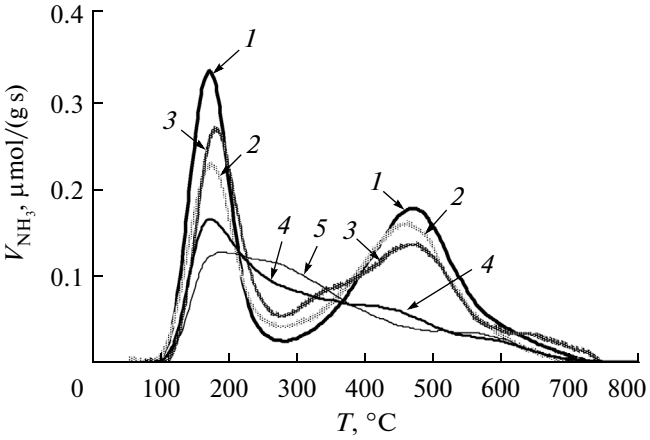

Fig. 1. NH_3 TPD curves for (*1*) MOR, (*2*) RM-1, (*3*) RM-2, (*4*) RM-3, and (*5*) MCM-41.

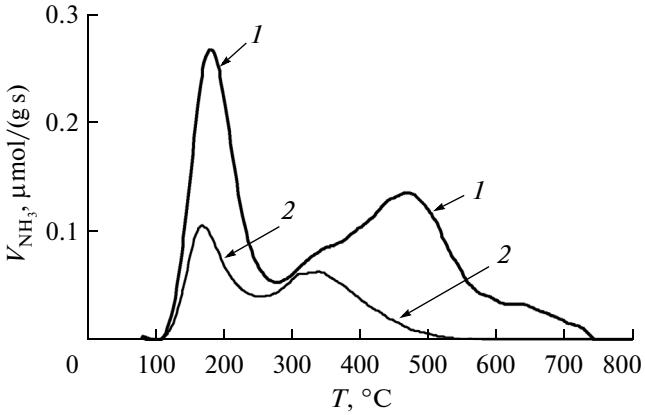

Fig. 2. NH_3 TPD curves for (*1*) RM-2 and (*2*) Cs/RM-2.

Figure 2 depicts NH_3 TPD curves for initial and cesium-modified RM-2. The spectra for samples RM-1 and RM-3 have the same pattern. It is seen that the introduction of cesium leads to a noticeable decrease in the number of acid sites.

The nature of acid sites was determined using the IR spectra of adsorbed pyridine (Py), which indicate the presence of Brønsted (1545 and 1637 cm^{-1}) and Lewis (1454 and 1622 cm^{-1}) acid sites in both initial mordenite and recrystallized samples (Fig. 3). The spectrum of pyridine adsorbed on sample RM-1 did not differ from that for initial mordenite (not presented in Fig. 3). As the degree of recrystallization increases, the total number of acid sites decreases, with the proportion of Lewis acid sites increasing. It is likely that the presence of Lewis acid sites in this case is due to partial cleavage of Si–O–Al bonds.

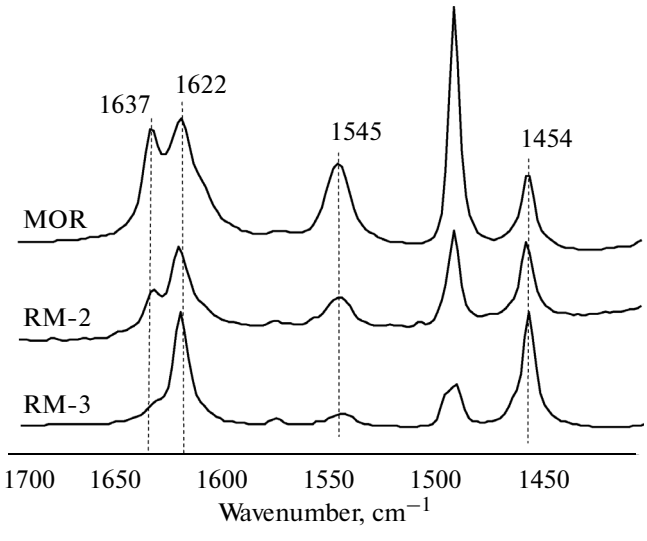

Fig. 3. IR spectra of pyridine adsorbed at 200°C on mordenite and micro–mesoporous samples RM-2 and RM-3.

Figure 4 presents the IR spectra of pyridine adsorbed at 200°C on the cesium-modified micro–mesoporous sample RM-2. It is seen that the introduction of cesium leads to a noticeable decrease in intensity of the peaks at 1545 and 1637 cm^{-1} due to Py adsorbed on Brønsted acid sites, with the intensity of the 1455-cm^{-1} band attributed to Lewis acid sites changing slightly. It is likely that ion exchange occurs during the impregnation with cesium acetate, and cesium occupies cation-exchangeable positions, a result that is consistent with the NH_3 TPD data.

Catalytic Properties

The catalytic properties of micro–mesoporous catalysts were examined in the conversion of acetone. The results are presented in Figs. 5 and 6 and in Table 2. The catalytic conversion of acetone leads to the formation of a wide range of products: mesityl oxide, acetic acid, methane, CO_2, C_2–C_4 light hydrocarbons, C_5–C_7 aliphatic hydrocarbons, and C_6–C_{10} aromatic hydrocarbons.

The catalytic properties of cesium-modified MOR, MCM-41, and micro–mesoporous catalysts were compared with regard to initial acetone conversion and isobutylene (desired product) formation rates (Fig. 5). The activity of the catalysts increases on passing from Cs/MOR to Cs/MCM-41. Since the total amount and strength of acid sites decreases in this order, the growth in the initial rate of acetone conversion is probably determined by the porosity characteristics of the material. Indeed, as the degree of recrystallization increases, the pore volume increases, thereby facilitating the diffusion of molecules and making catalyst active sites more accessible. The increase in the initial rate of isobutylene formation on passing from Cs/MOR to Cs/MCM-41 suggests that its formation can occur on both Brønsted and Lewis acid sites, since noticeable decrease in the amount Brønsted sites and an increase in the amount of Lewis

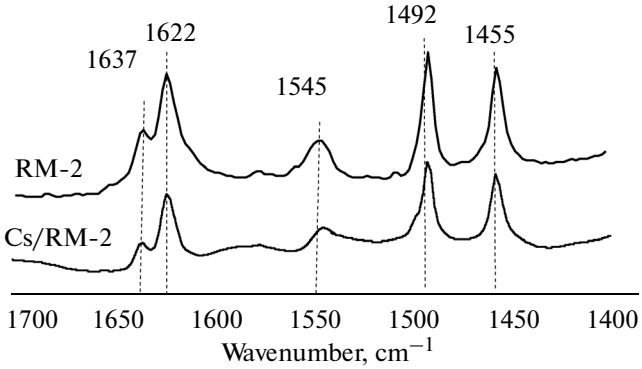

Fig. 4. IR spectra of pyridine adsorbed at 200°C on RM-2 and Cs/RM-2.

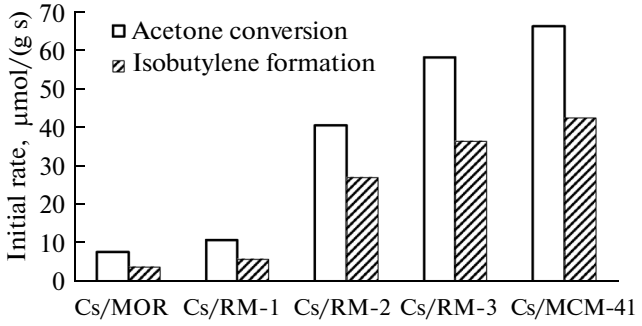

Fig. 5. Initial rates of acetone conversion and isobutylene formation over initial MOR and MCM-41 and the cesium-modified micro–mesoporous materials.

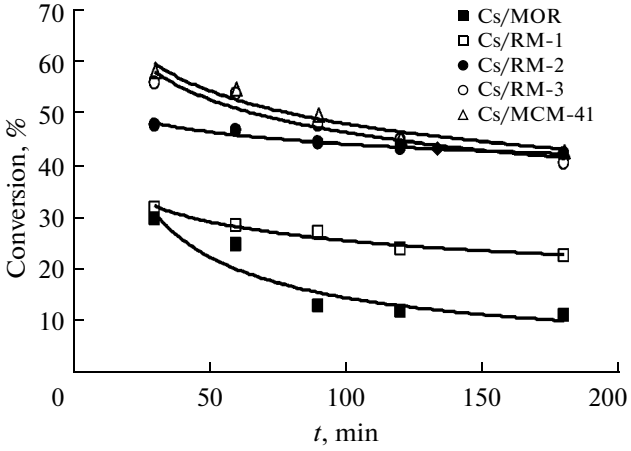

Fig. 6. Conversion of acetone at 500°C and WHSV = 2 h^{-1} as a function of time for MOR, MCM-41, and cesium-modified recrystallized samples

sites with the increasing degree of recrystallization are observed.

The parameters of catalytic activity of Cs-containing micro–mesoporous catalysts at 500°C and an acetone WHSV of 2 h^{-1} are collated in Table 2. An increase in the degree of recrystallization of the samples leads to the growth in the conversion of acetone, a finding that is consistent with the data on the initial acetone conversion rates. Note that the selectivities for the desired product isobutylene, acetic acid, and methane decrease, the CO_2 selectivity changes slightly, and the selectivity for aromatic and C_2–C_4 hydrocarbons increases with an increase in the proportion of mesopores in the samples. The decline in the selectivity for isobutylene with an increase in the degree of recrystallization of the samples can be associated either with the fact that Brønsted acid sites, which are in a greater amount in mordenite and weakly recrystallized RM-1, are more preferable for the formation of isobutylene than Lewis acid sites or with the fact that at longer contact times in wide pores of micro–mesoporous aluminosilicates RM-3 and MCM-41, a preferred route of acetone conversion is the condensation of three or more acetone molecules, which can further transform into aromatic molecules through dehydrocondensation. In addition, the enhancement of selectivity for C_3–C_5 hydrocarbons in the order Cs/MOR–Cs/MCM-41 allows the conclusion that the isobutylene produced undergoes dimerization followed by decomposition into propylene and pentane.

The best performance in the isobutylene production from acetone was shown by Cs/RM-3, the yield of isobutylene on which was 31.5 wt %.

Figure 6 presents a comparison of data on the time-on-stream stability of Cs-containing catalysts. It is worth noting that all the catalysts are deactivated with

Table 2. The conversion of acetone and selectivity of formation of the products of the reaction of transformation of acetone over the following catalysts: MOR, MCM-41, and Cs-modified micro--mesoporous aluminosilicates; 500°C, 2 g/(g h)

Catalyst	Cs/MOR	Cs/RM-1	Cs/RM-2	Cs/RM-3	Cs/MCM-41
Conversion, %	35.5	34.4	44.7	56.2	58.4
		Selectivity, wt %			
Isobutylene	63.9	63.9	54.1	55.1	40.6
Methane	2.2	1.2	1.3	1.2	1.5
Ethylene	0.2	0.1	0.1	0.1	0.4
Ethane	0.0	0.0	0.0	0.0	0.1
CO_2	26.7	25.0	28.2	33.5	29.7
Propylene	2.6	2.1	3.4	3.4	7.1
C_4	1.8	1.9	4.8	2.2	8.2
C_5–C_7	1.2	1.8	2.0	1.8	3.1
Aromatic hydrocarbons	1.2	4.7	5.8	2.7	9.2
Acetic acid	0.2	0.4	0.0	0.0	0.0
Isobutylene yield, wt %	22.7	22.0	24.2	31.5	23.7

time, with the selectivity for isobutylene remaining almost unchanged over time. The micro–mesoporous materials are more stable than mordenite. The cause of the substantial deactivation of the zeolite catalyst can be both the presence of strong Brønsted acid sites, which actively mediate coking processes, and a small size of pores, which are blocked by condensation products.

Thus, recrystallization leads to the creation of transport pores and an increase in the accessibility of active sites, thereby enhancing the activity of such catalysts in the conversion of acetone into isobutylene. Micro–mesoporous materials operate more stably as compared to mordenite.

ACKNOWLEDGMENTS

This work was supported by the Russian Science Foundation, project no. 14-23-00094.

REFERENCES

1. T. Tago, H. Konno, M. Sakamoto, et al., Appl. Catal., A **403**, 183 (2011).
2. A. N. Shuikin, L. G. Liberov, R. A. Fridman, et al., Neftekhimiya **17**, 715 (1977).
3. M. Demorest, D. Mooberry, and J. D. Danforth, Ind. Eng. Chem. **43**, 2569 (1951).
4. A. J. Crisci, H. Dou, T. Prasomsri, and Y. Roman-Leshkov, ACS Catal. **4**, 4196 (2014).
5. Y. Hirota, Y. Nakano, K. Watanabe, et al., Catal. Lett. **142**, 464 (2012).
6. G. J. Hutchings, P. Johnston, D. F. Lee, et al., J. Catal. **147**, 177 (1994).
7. T. Tago, H. Konno, S. Ikeda, et al., Catal. Today **164**, 158 (2011).
8. G. J. Hutchings, P. Johnston, D. F. Lee, and C. D. Williams, Catal. Lett. **21**, 49 (1993).
9. A. J. Cruz-Cabeza, D. Esquivel, C. Jimenez-Sanchidrian, and F. J. Romero-Salguero, Materials **5**, 121 (2012).
10. L. Kubelkova and J. Novakova, Appl. Spectrosc. **11**, 822 (1991).
11. O. Kikhtyanina, V. Kelbichovaa, D. Vitvarovab, et al., Catal. Today **227**, 154 (2014).
12. C. D. Chang and A. J. Silvestri, J. Catal. **47**, 249 (1977).
13. S. Slamet and M. Nasikin, Int. J. Eng. Technol. **11** (2), 72 (2011).
14. C. Velosoa, J. Monteiroa, and E. Sousa-Aguiarb, Zeolites Relat. Microporous Mater. **84**, 1913 (1994).
15. H. Kossilick, G. Lischke, B. Parlitz, W. Storek, R. Fricke, Appl. Catal., A **184**, 49 (1999).
16. G. S. Salvapati, K. V. Ramanamurty, and M. Janardanaro, J. Mol. Catal. **54**, 9 (1989).
17. I. I. Ivanova and E. E. Knyazeva, Chem. Soc. Rev. **42**, 3671 (2013).
18. V. V. Ordomsky, I. I. Ivanova, E. E. Knyazeva, et al., J. Catal. **295**, 207 (2012).

Translated by E. Boltukhina